A Novel Submillimeter-Wave Detector Using Quantum Point Contacts

Qing Hu, R.A. Wyss, C.C. Eugster, J.A. del Alamo, S. Feng†, M.J. Rooks,††
and M.R. Melloch†††

Department of Electrical Engineering and Computer Science and Research Laboratory of Electronics, MIT, Cambridge, MA 02139
†Department of Physics, University of California at Los Angeles
††National Nanofabrication Facility, Cornell University
†††Department of Electrical Engineering, Purdue University

Abstract

We are developing a novel submillimeter-wave and THz detector using semiconductor quantum point contacts. The operation principle of this unique device is based on a new physical phenomenon, called *photon-assisted quantum transport*,[1] in which photons enhance the energy of ballistic transport electrons and produce a photon-induced drain/source current.

A quantum point contact is formed by depleting the 2DEG (two-dimensional electron gas) underneath a split-gate electrode on a MODFET (modulation-doped field-effect transistor) structure. For our device, the split-gate also serves as the two terminals of a planar antenna which concentrates the radiation field in the point contact region. The electrical field of the radiation near the split-gate is orthogonal to the drain/source conduction path. Intersubband transitions can therefore be excited that contribute to the drain/source conduction. It is estimated in our theory that the current responsivity of the quantum point contact detectors can be comparable to the quantum efficiency $e/\hbar\omega$ at and above 1 THz. The capacitance of this device should be small due to the planar geometry. Thus, the RC roll-off, which is inevitable in all tunnel devices such as SIS junctions and Schottky diodes, is negligible. Consequently, a very high-frequency quantum photon detector ($\geq$1 THz) could be developed.

We have fabricated several quantum point contacts with antenna/split-gate structures using a combination of optical and electron-beam lithography on a GaAs/AlGaAs MODFET structure with a 2D electron density 2.8×10^{11} cm^{-2}, and an electron mobility 200,000 cm^2/V•sec at 45 K. Under a 300 GHz coherent radiation at about 0.5 mW level, a profound photon-induced drain/source current is produced throughout the entire gate voltage region in which the quantum point contact exhibits the behavior of an 1D electron system. The amplitude of the photon-induced current is comparable to that corresponding to a quantized conductance step, i.e. $(2e^2/h)V_{DS}$, and it oscillates with the gate voltage. Our analysis suggests that the photon-induced drain/source current is mainly due to heating (or a bolometric effect). Future improvement of device parameters are discussed.

I. Introduction

Ballistic quantum transport through semiconductor quantum point contacts has been an active research area in recent years. In essence, such devices are made of very clean two-dimensional electron gas samples with a finely structured split gate on the wafer surface. Thus at low temperatures, electrons can travel from the source to drain without suffering elastic and inelastic scattering. This results in the well-known quantized drain/source conductance behavior, with a conductance quantum of $2e^2/h$.[2,3] Extensive work has been done after the discovery of this effect to study various features and extensions of this novel quantum transport device.[4] However, most of the experiments that have been performed on such devices are limited to DC transport measurements.

It is well known in the field of superconducting tunneling that photons can assist the tunneling process, provided that tunneling is elastic so that electrons do not suffer inelastic scattering.[5] The theoretical framework for photon-assisted tunneling has been well established and verified in experiments. The effect of photon-assisted tunneling has also been utilized in heterodyne receivers and radiation detectors using superconducting tunnel junctions. These devices have been demonstrated superior to other devices in terms of sensitivity and speed.[5] In a broad sense, elastic tunneling is a phase-coherent quantum transport in a classically forbidden region. Therefore, the results of photon-assisted tunneling can be applied to the study of photon-assisted quantum transport in semiconductor devices. If demonstrated successfully, novel devices based on the photon-assisted quantum transport can be developed for applications in the THz frequency range where very few devices are available.

II. Theory of Photon-assisted Quantum Transport

We consider a standard split-gate quantum point contact device, as shown in Fig. 1. The electrons are confined to two-dimensional movements at the interface of a GaAs/AlGaAs modulation-doped heterojunction. We assume that the 2D electron gas has a high mobility so that no impurity potential near the constriction region needs to be included in our calculation. Two capacitive split gates are patterned on top of the device, which form the constriction for the point contact device. The shape of the split gates can be described by the distance between them, D(x), where the x-direction is that of electron transport. Application of a negative gate voltage $-V_G$ creates subband structures in the direction perpendicular to transport (the y-direction in Fig. 1). We model the effect of this negative gate voltage on the electron gas underneath by an effective channel width of the electron gas, $d(x) \leq D(x)$, which decreases with an increasing negative gate voltage. We also assume that the variation of d(x) is slow enough so that WKB-type adiabatic semiclassical approximations for the electron wave function can be applied. Within this approximation, assume infinite potential sidewalls at $y = \pm d(x)/2$, the electron eigenstates $\psi_n(x,y)$ can be expressed as products of the longitudinal (in the x

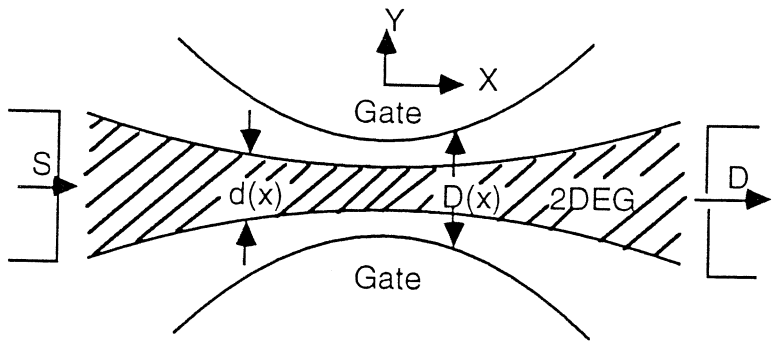

Figure 1 Geometry of the quantum point contact device under consideration. Under a negative gate voltage, electrons travel from the source (S) to the drain (D) through a channel with an x-dependent width d(x).

direction) eigenfunctions $\phi_n(x)$ and the transverse (in the y direction) standing-wave functions $\chi_n(y)$, where

$$\chi_n(y) = \sin[\frac{n\pi y}{d(x)}] , \qquad n \text{ even},$$

$$\chi_n(y) = \cos[\frac{n\pi y}{d(x)}] , \qquad n \text{ odd}, \tag{1}$$

with transverse eigenenergies given by

$$E_n(x) = \frac{n^2\pi^2\hbar^2}{2md(x)^2} . \tag{2}$$

This gives rise to the familiar subband structures so that the subband potential energies increase to their maximum values at the narrowest point of the constriction, i.e. x = 0 in Fig. 1. By substituting $\psi_n(x,y)$ in the time-independent Schrödinger equation, we reduce the original two-dimension equation into one-dimensional equations,

$$[-\frac{\hbar^2}{2m}\frac{d^2}{dx^2} + E_n(x)]\phi_n(x) = E\phi_n(x) . \tag{3}$$

Eq. (3) implies that the electrons in the nth subband are subject to a potential $E_n(x)$. The first few $E_n(x)$'s are sketched in Fig. 2(a). Using WKB approximation, electrons with energies greater than the potential barrier $E_n(0)$ will have a unity transmission coefficient from the source to the drain, while electrons with energies less than $E_n(0)$ will have a zero transmission coefficient. As the electron Fermi energy increases, more subbands will be turned on. Since each subband contributes exactly $2e^2/h$ to the drain/source conductance,[6] the total conductance of the device will increase discontinuously as the Fermi energy (or equivalently, the gate voltage) increases. This results in the well-known step structures of the drain/source conductance G_{DS} vs. the gate voltage V_{GS} curves.

The novel idea of photon-assisted quantum transport is to use far-infrared photons to enhance the energies of the 2-D electron gas in the source, so that they will be energetic enough to pass through the subbands and contribute to conduction. A schematic illustrating the idea is shown in Fig. 2(a). In this picture, the electron waveguide is pinched off so that the Fermi level lies below the energy barrier $E_n(0)$ of the n = 1 subband. Radiation photons increase the energy of electrons, so they can travel over the barrier $E_1(0)$. This photon-assisted transport will result in a photon-induced drain/source current. This idea is similar to photon-assisted tunneling in superconducting tunnel junctions. In photon-assisted tunneling, quasiparticle electrons in the valence band on one side of a junction absorb photons to enhance their energy, and subsequently tunnel to the conduction band on the other side of the junction. Because of this similarity, we call the possible photoelectric effect of the conduction through a quantum point contact "photon-assisted quantum transport."

In the presence of radiation, the total Hamiltonian will have a time-dependent component. For simplicity, here we will only consider the case in which the radiation field is in the y direction (the transverse case). The results for the longitudinal case (**E** field in the x direction) is similar to the transverse case, but the mathematics is more complicated.[7] For the transverse case, the time-dependent Hamiltonian is

$$H' = -eE_{ac}y\cos(\omega t) . \tag{4}$$

From selection rules, H' will couple subbands with opposite parities. Thus, intersubband transitions will occur. In general, the solutions of the time-dependent Schrödinger equation should include all the subband wave functions, that is,

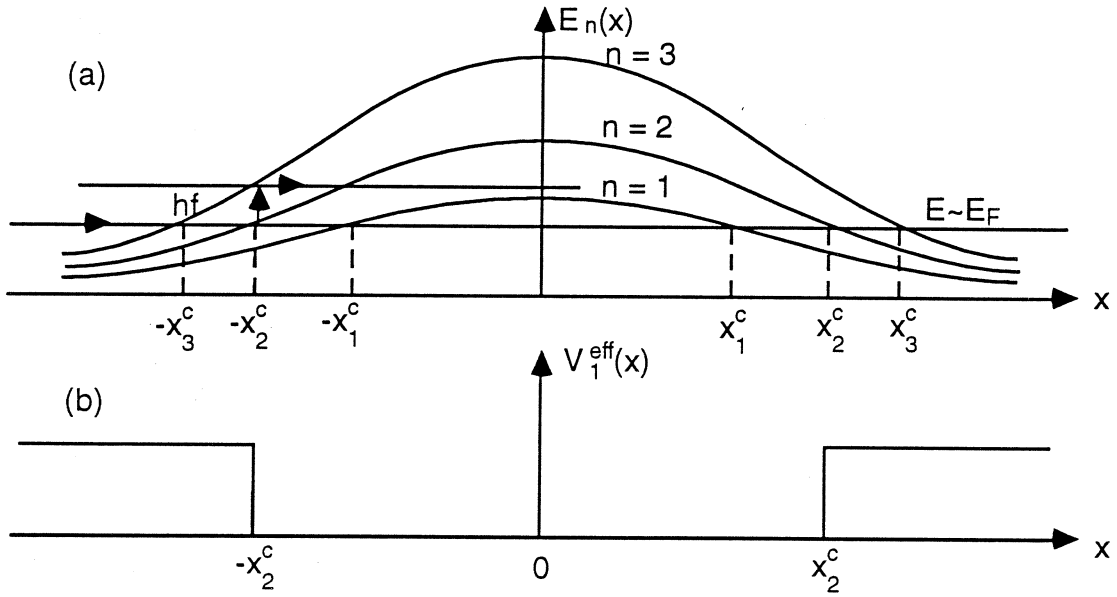

Figure 2 (a) Effective one-dimensional potential profile for the transport electrons moving from the source to drain in a quantum point contact. The barrier potential arises from the subband energies $E_n(x)$, which is x dependent (cf. Eq. (2)). Electrons from a particular subband n can propagate adiabatically through the point contact if the electron energy $E \sim E_F$ is greater than the maximum barrier height $E_n(0)$. Under radiation, electrons with energies even less than $E_n(0)$ can propagate over the barriers by absorbing an integer number of photons, as illustrated in the figure. (b) Effective AC potential V_1^{eff} for the electrons in the first subband.

$$\psi(x,y,t) = \sum_n C_n(x,t)\phi_n(x)\chi_n(y) , \tag{5}$$

and

$$[-\frac{\hbar^2}{2m}(\frac{\partial^2}{\partial x^2}+\frac{\partial^2}{\partial y^2}) - eE_{ac}(x)y\cos\omega t]\,\psi(x,y,t) = i\hbar\frac{\partial\psi(x,y,t)}{\partial t} . \tag{6}$$

We are most interested in electrons in the first subband where the dc potential barrier is the lowest. Multiplying Eq. (6) by $2\chi_1(y)/d$ and then integrating over y from -d/2 to d/2 leads to:

$$[-\frac{\hbar^2}{2m}\frac{\partial^2}{\partial x^2} + E_1(x)]\phi_1(x,t)C_1(x,t) - eE_{ac}(x)\cos\omega t \sum_{n\geq 2} D_{1n}C_n(x,t)\phi_n(x) = i\hbar\phi_1(x)\frac{\partial C_1(x,t)}{\partial t} , \tag{7}$$

where

$$D_{1n} = \frac{2}{d(x)}\int_{-d/2}^{d/2} y\chi_1(y)\chi_n(y)dy .$$

Eq. (7) is the equation of motion for the component of the electron wavefunction in the first subband, which is coupled via "dipole" moment D_{1n} to those of higher subbands with an odd parity.

The subband that mixes with the first subband most is the second subband, with a "dipole" moment given by

$$D_{12}(x) = \frac{2}{d(x)}\int_{-d/2}^{d/2} y\cos(\pi y/d(x))\,\sin(2\pi y/d(x))dy = \frac{16d(x)}{9\pi^2} \approx 0.2d(x).$$

The next subband that mixes with the first subband is the fourth subband. As the dipole moment D_{1n} decays rapidly with n (for example, $|D_{14}| = \frac{2}{25}D_{12}$), we can then make a further simplification by concentrating on the D_{12} term only, and. Eq. (7) then reduces to the form

$$[-\frac{\hbar^2}{2m}\frac{\partial^2}{\partial x^2} + E_1(x) + V_1^{eff}(x,t)]\psi_1(x,t) = i\hbar\frac{\partial\psi_1(x,t)}{\partial t}, \qquad (8)$$

where we have rewritten $\psi_1(x,t) = \phi_1(x)C_1(x,t)$, and have introduced an effective time-dependent perturbation potential

$$V_1^{eff} = -eD_{12}(x)E_{ac}(x)\cos(\omega t)\frac{\phi_2(x)C_2(x,t)}{\phi_1(x)C_1(x,t)} \approx -0.2eV_{ac}\frac{d(x)\,\phi_2(x)}{D(x)\,\phi_1(x)}\cos\omega t, \qquad (9)$$

where $V_{ac} = E_{ac}(x)D(x)$. In Eq. (9), we have approximated the two C-functions to be the same, which is certainly valid in regions far away from the classical turning points x^c. Therefore, V_1^{eff} is mainly determined by the ratio of the wave functions of the two subbands $\phi_2(x)$ and $\phi_1(x)$.

Thus, with suitable approximations, we can map the photon-assisted transport problem in the transverse case into an effective one-dimensional Schrödinger equation with an AC and a DC potential. Since $\phi_1(x) \approx \phi_2(x)$ in regions far away from the classical turning point of the second subband x_2^c (x_2^c is shown in Fig. 2(a)), the amplitude of the AC potential V_1^{eff} is approximately constant in the region $|x| > x_2^c$, and V_1^{eff} decreases exponentially for $|x| < x_2^c$. Thus to a good approximation, we can treat V_1^{eff} as a piece-wise potential with $V_1^{eff} = 0.2eV_{ac}d(x_2^c)/D(x_2^c)$ for $|x| \geq x_2^c$, and $V_1^{eff} = 0$ for $|x| < x_2^c$, as shown in Fig. 2(b).

Using this piece-wise ac potential V_1^{eff}, in the region where $|x| < x_2^c$ the solution of the Schrödinger equation is the same as the one without radiation. While in the region $|x| \geq x_2^c$, since V_1^{eff} is spatially independent, the spatial part of the wave functions remains the same while the temporal part of the wave functions has an additional phase factor[8]

$$\exp[i(eV_1^{eff}/\hbar\omega)\sin\omega t] = \sum_{n=-\infty}^{\infty} J_n(\alpha)e^{-in\omega t}, \qquad (10)$$

where J_n is the nth order Bessel function, and $\alpha = eV_1^{eff}/\hbar\omega$ is a dimensionless parameter which is proportional to the strength of the radiation field.

Eq. (10) implies that the new wave function has components with energies $E+n\hbar\omega$. Physically this means that the photon field creates new eigenstates with energies $E+n\hbar\omega$. Positive n's correspond to states where electrons have absorbed n photons, while negative n's correspond to states where electrons have emitted n photons. The amplitude of these new eigenstates is $J_n(\alpha)$, and the corresponding electron density is $J_n^2(\alpha)$.

For a simple situation, consider a bias condition where the Fermi energy E_F is suppressed at $\leq\hbar\omega$ below the first subband $E_1(0)$ of the quantum point contact, as shown in Fig. 2(a). Then the occupancy of states at $E_1(0)$ is zero at T = 0, and so is the drain/source current in the absence of radiation. In the presence of the radiation, however, there will be occupied states at $E \geq E_1(0)$, with an occupancy of $J_1^2(\alpha)$ due to one-photon absorption, and $J_n^2(\alpha)$ due to n-photon absorption. Since a fully occupied subband contributes a drain/source conductance $(2e^2/h)$, these partially occupied states will contribute to a photon-induced current of $(2e^2/h)V_{DS}\sum_{n=1}^{\infty} J_n^2(\alpha) = [1 - J_0^2(\alpha)](e^2/h)V_{DS}$, which has a maximum value of $(e^2/h)V_{DS}$. Thus, the photon-induced current

from the first subband is maximally half of the current at the first conductance step. The total photon-induced current will be the sum of the contributions from all the subbands. In the small signal limit, $\alpha << 1$, only J_1 is significant and $J_1^2(\alpha) \approx \alpha^2$, then the photon-induced current will be proportional to the square of the **E** field, or the power of the radiation. This results in a square-law or video detection. When $\alpha >> 1$, higher order Bessel functions in Eq. (10) become more important, which implies that multiphoton (or nonlinear) processes become dominant.

The situation for E_F being at $> \hbar\omega$ below $E_1(0)$ is similar to the case discussed above, except a multiphoton absorption is now required for the photon-assisted transport. Therefore, it is less efficient. The photon-induced current for a gate voltage just above the pinch off should be negative, due to a depletion of the occupied subband. In general, at frequencies much higher than the thermal broadening $3.5\ k_BT$, a coherent far-infrared radiation will produce ministep structures in G_{DS} vs. V_{GS} curves, as shown in Fig. 3. The width of the ministep is proportional to the frequency, and the height of the ministeps is a function of the radiation power in the form of

$$(2e^2/h)V_{DS}\sum_{n}^{\infty} J_n^2(\alpha). \qquad (11)$$

The lower limit of the summation is determined by the difference between $E_n(0)$ and E_F relative to the photon energy $\hbar\omega$.

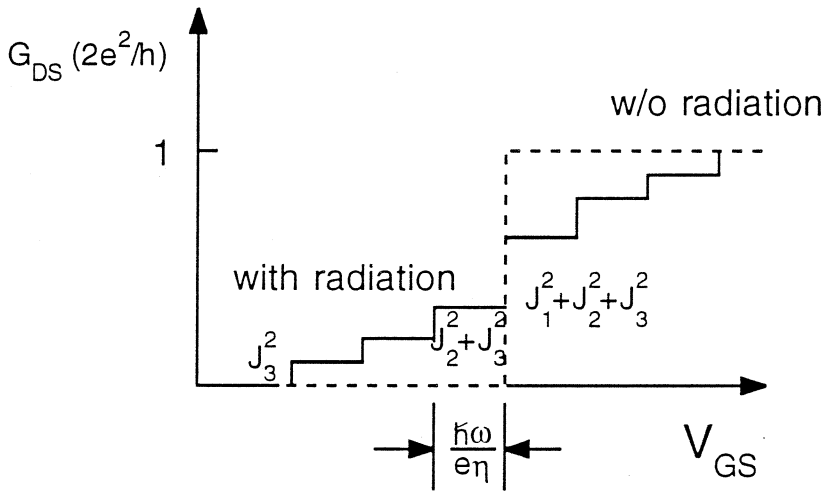

Fig. 3 Predicted G_{DS} vs. V_{GS} curves of a quantum point contact under a coherent far-infrared radiation. The range of the gate voltage is around the onset of the first conductance step. η is a dimensionless factor which is determined by the geometry of the quantum point contact which relates the gate voltage to the energy level of the subbands.

III. Preliminary experimental results

Two important technical issues need to be addressed in order to observe the effect of photon-assisted quantum transport. The first one is the required frequency range of the far-infrared radiation, and the second is how to couple this long-wavelength radiation to a quantum point contact with submicron dimensions.

At a finite temperature T, the thermally excited electrons can also contribute to a drain/source current below the pinch-off threshold. In order to observe a profound photon-induced drain/source current, the photon energy must be much greater than the thermal broadening of the Fermi surface $3.5\ k_BT$,[9] where k_B is the Boltzmann constant. At 1.5 K, which is the temperature of a typical helium cryostat with far-infrared access ports, $3.5\ k_BT/h \approx 100$ GHz. Thus, a submillimeter-wave radiation source at ≥ 300 GHz should provide sufficiently energetic photons to

assist the drain/source transport. A CO_2 laser-pumped far-infrared laser should provide the required radiation. Solid-state sources, such as Gunn oscillator-pumped Schottky-diode multipliers, are also adequate sources at frequencies below 500 GHz.

In order to couple far-infrared radiation (whose wavelength is typically on the order of 1 millimeter) to the quantum point contact of submicron size, a planar antenna[10] is required to concentrate the radiation field into the area where the drain/source conduction takes place. Otherwise, most of the radiation will bypass the quantum point contact. In addition, to excite the intersubband transitions, the **E** field of the radiation should be polarized in the direction transverse to the drain/source conduction path. This can be achieved by placing the antenna in such a way that its terminals also serve as the split-gate electrodes, as shown in Fig. 4(a). The radiation electric field at the antenna terminals is perpendicular to the antenna terminals, as shown in Fig. 4(b), which is roughly perpendicular to the drain/source conduction path.

It is advantageous to use broadband antennas so that radiation in a broad frequency range can be coupled to the quantum point contact in order to perform spectroscopy. One family of broadband antennas is the self-complementary antenna, in which the pattern of the metal part is the same as the dielectric part.[10] According to Booker's theorem,[10] the impedance of a self-complementary antenna is independent of frequency. The simplest self-complementary antenna is a 90^o bow-tie antenna, as shown in Fig. 4. Its wedge-shaped electrodes can also help to make the electron transport through the quantum point contact adiabatic.

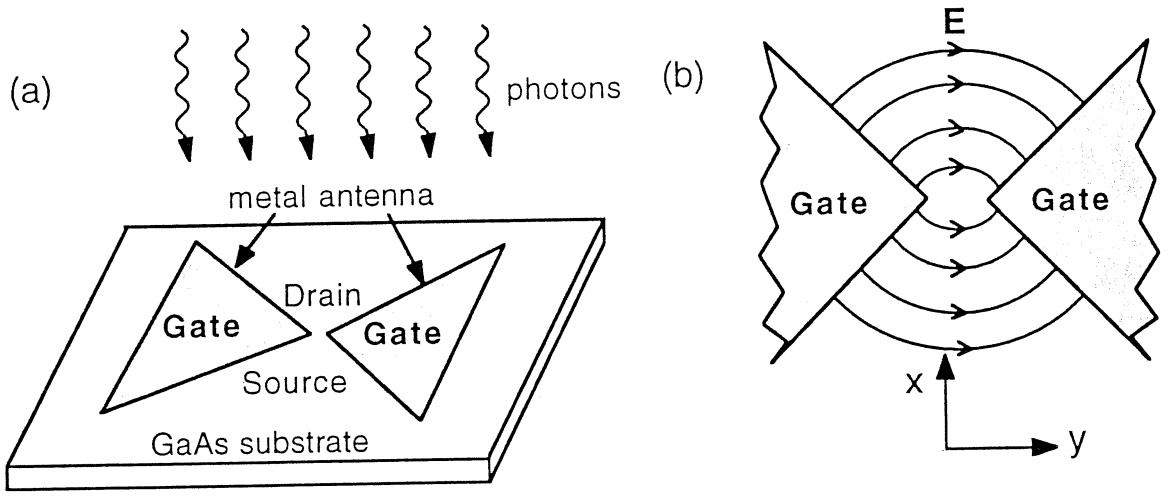

Fig.4 (a) An antenna-coupled quantum point contact. The planar antenna concentrates the radiation field into the small gap region between the two antenna terminals. (b) Central region in (a), the curved lines are the electric field of the radiation near the antenna/gate terminals.

We have successfully fabricated several quantum point contacts which are coupled with planar antennas. The fabrication was made using a combination of optical and electron-beam lithography on a GaAs/AlGaAs MODFET structure with a two-dimensional electron density $N = 2.8\times10^{11}$ cm^{-2}, and an electron mobility μ = 200,000 $cm^2/V\cdot sec$ at 45 K. The electron-beam lithography was performed at the National Nanofabrication Facility at Cornell University.[11] SEM pictures of one of the devices with a log-periodic antenna (it is also self-complementary but it has a better antenna pattern than that of bow-tie antennas) is shown in Fig. 5. The gate electrodes are shaped like 45^o wedges, and the opening of the split-gate is 0.15 μm.

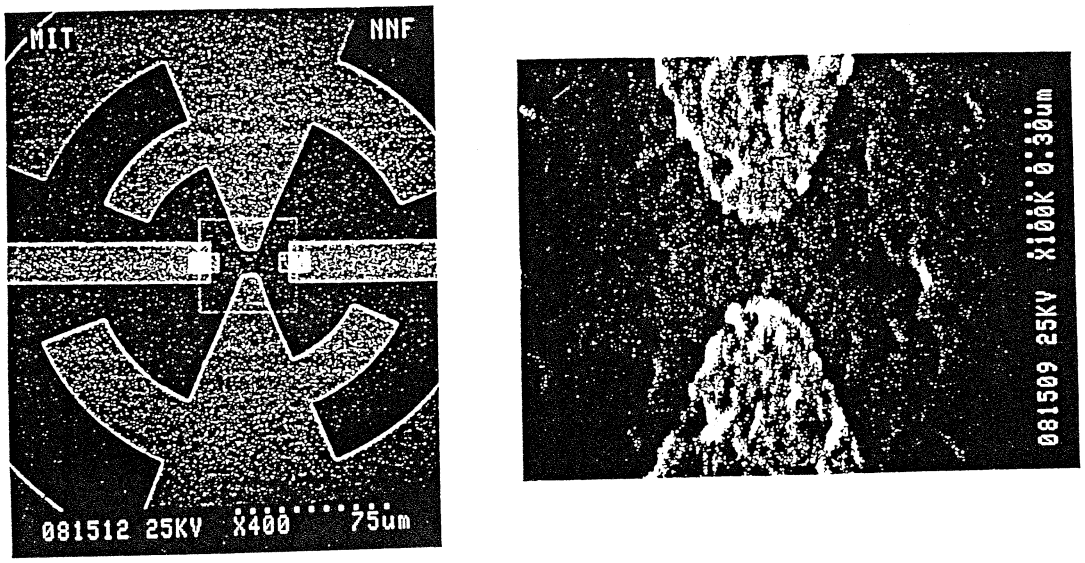

Fig. 5 SEM of a quantum point contact with a log-periodic antenna. The opening of the split-gate is 0.15 μm.

The measurement was performed in a cryostat in which the device is submerged in liquid helium. By pumping the helium bath, the device can be cooled down to 1.5 K. The cryostat has a quartz window with a low-pass black polyethylene filter which allows the pass of far-infrared radiation, and cuts off at frequencies above several THz. Extreme care was taken to minimize the ground-loop pick-up noise and to filter out undesired RF signals. Using a special home-made electronic bias circuit and amplifier, we were able to measure the voltage signals at levels below one microvolt and the current signals at levels below one nanoampere. For a quick measurement of the drain/source current as a function of voltage, we can apply a dc drain/source voltage of 150 μV and sweep the gate voltage at several ten Hz. The measured I_{DS}-V_{GS} curves is displayed on an oscilloscope, as shown in Fig. 6(a).

The I-V curve measurement can also be made using a digitally controlled voltage supply to sweep the gate voltage. The drain/source current is measured using a lock-in technique. In this way, the data can be collected by a computer and easily analyzed. Fig. 6(b) shows the drain/source conductance as a function of the gate voltage. Fifteen conductance steps are clearly seen which indicates the high quality of the device. The deviation from $n(e^2/h)$ at higher steps is due to the series resistance, which becomes more important at higher steps where the device is more conducting.

The radiation source is a tunable (75-110 GHz) Gunn oscillator-pumped Schottky frequency tripler with output frequencies at about 300 GHz. The maximum output power is 0.5 mW. The radiation beam of the frequency tripler is launched into free space through a conical horn, and then focused through the window of the cryostat by two TPX lenses. The radiation signal reaches the device from the air side of the planar antenna. At the maximum radiation power level, a profound photon-induced drain/source current is produced throughout the entire gate voltage region where the quantum point contact exhibits the behavior of a 1-D electron system. The amplitude of the photon-induced current is comparable to that corresponding to a quantized conductance step, i.e. $(2e^2/h)V_{DS}$, and it oscillates with the gate voltage, as shown in Fig. 7.

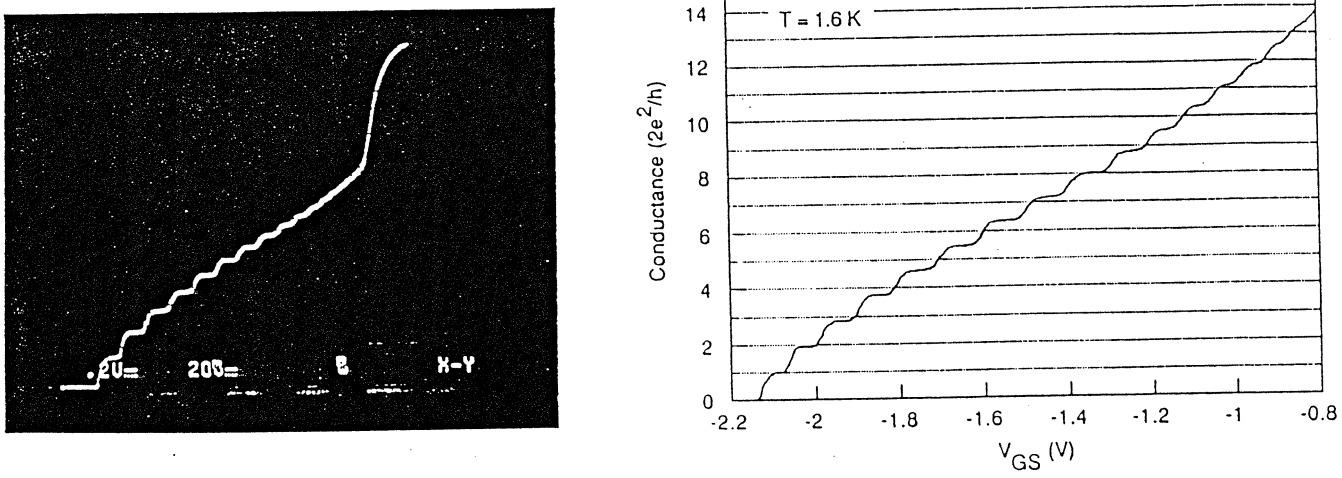

(a) (b)

Fig. 6 (a) Drain/source current as a function of the gate voltage. (b) Drain/source conductance as a function of the gate voltage.

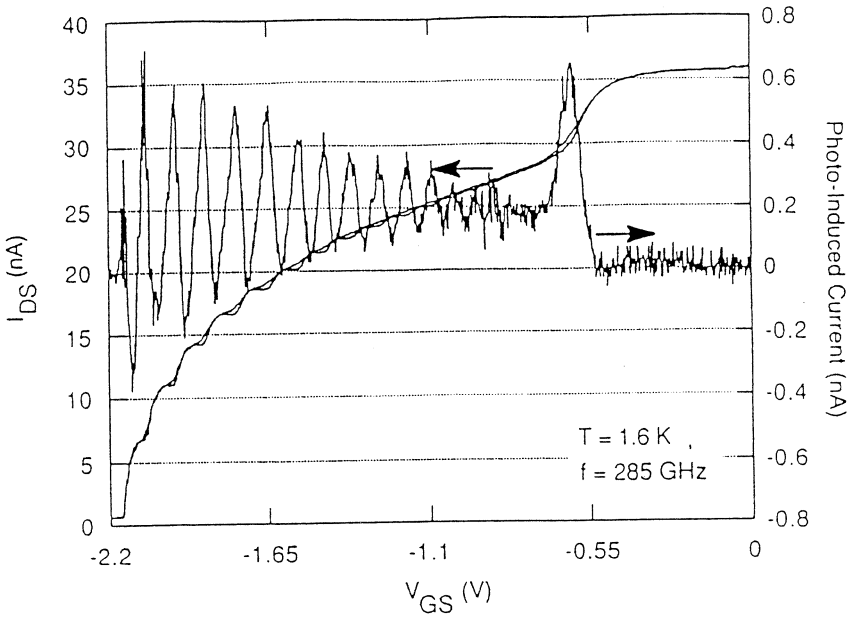

Fig. 7 Drain/source current vs. the gate voltage with and without the far-infrared radiation. The difference between the two currents is the photon-induced current, which is the oscillatory curve.

In order to compare our measurement with the theoretical predictions shown in Fig. 3, we plot the photon-induced drain/source current and the drain/source conductance measured without radiation as functions of gate voltage in a range where the conductance step structures are sharp, as shown in Fig. 8. The photon-induced current is mainly positive below the threshold of the next conductance step, and negative above the threshold of the step. This behavior qualitatively

resembles the prediction from our theory of photon-assisted quantum transport. However, no ministep structures such as those shown in Fig. 3 were seen in our measurement.

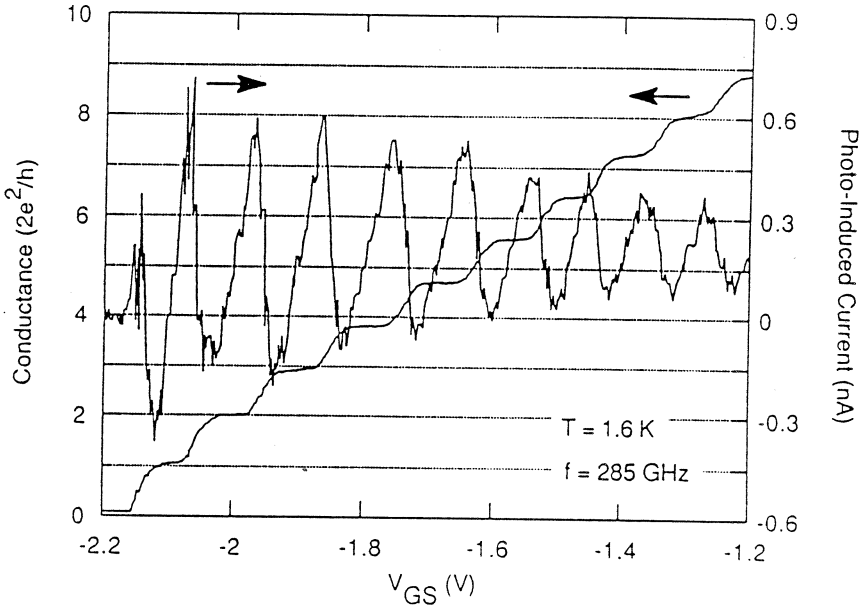

Fig. 8 Drain/source conductance and the photon-induced current as functions of the gate voltage. The photon-induced current is mainly positive below the threshold of the next conductance step and mainly negative above the threshold.

The mostly likely cause of the observed far-infrared photon-induced drain/source current is the heating of the 2DEG by the far-infrared radiation. The absorbed far-infrared radiation energy increases the temperature of the electron gas and the surrounding area, so the local temperature is higher than the temperature of the liquid helium bath. This higher local temperature broadens the Fermi surface and produces an additional drain/source current . To verify this hypothesis, we plot the difference between the drain/source current taken at 3.7 K and 1.6 K (without radiation) as a function of the gate voltage in Fig. 9. It appears quite similar to that shown in Fig. 7. Thus, this measurement supports our preliminary conclusion that the observed photon-induced drain/source current is mainly due to heating.

Our preliminary measurement and analysis then raise a difficult issue for experimentally observing the effect of photon-assisted quantum transport. Unlike photon-assisted tunneling in superconducting tunnel junctions, where the superconducting energy gap prevents energy absorption in the leads below the gap frequency, the excitation in the 2-D electron gas in a quantum point contact is, however, gapless. Thus, absorption can occur anywhere in the 2DEG, and the effect of the photon-assisted quantum transport will always be accompanied by a heating effect. In our devices, the effect of photon-assisted quantum transport is suppressed due to a device defect which was realized only recently: the central part (~10 μm) of the split-gate/antenna terminals is made of a 200 Å-thick gold film using e-beam lithography and lift-off techniques. This thickness is much thinner than the skin depth at 300 GHz (which is about 1000 Å), thus the 200 Å-thick antenna terminals are rather resistive. Therefore, as illustrated in Fig. 10, most of the radiation electric field drops within the antenna terminals instead of between them, where a strong radiation electric field is required to excite the intersubband transitions. Thus, most of the absorbed far-infrared radiation energy is consumed in increasing the temperature of the 2DEG, instead of in assisting the quantum transport processes.

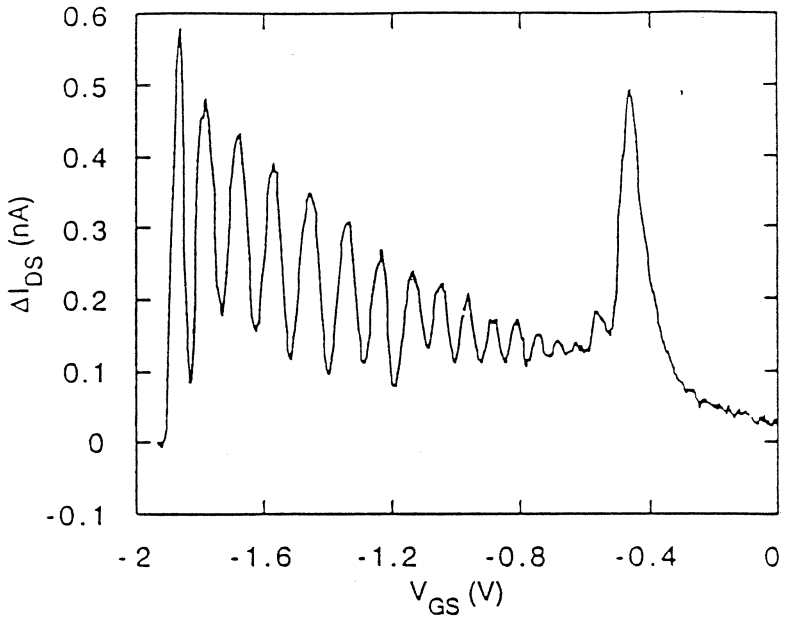

Figure 9 Thermally induced drain/source current (which is defined as the difference between the drain/source current measured at 3.7 K and 1.6 K) as a function of the gate voltage. It exhibits similar behavior as the photon-induced drain/source current, as shown in Fig. 7.

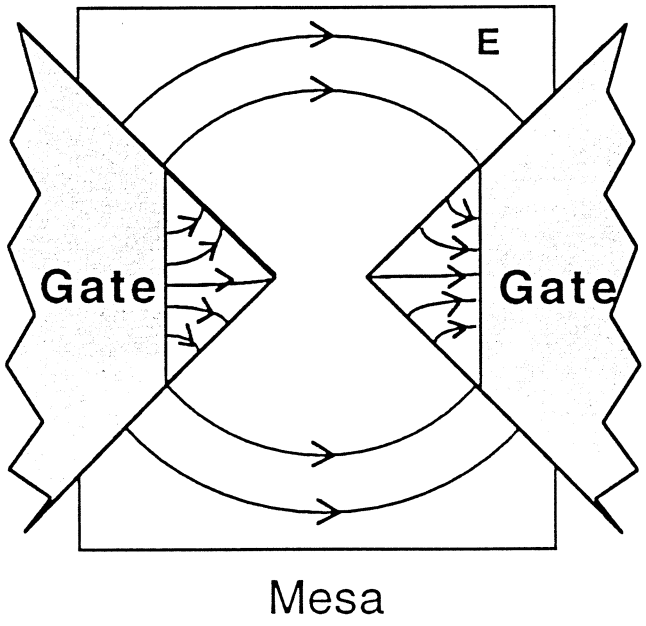

Fig. 10 Radiation electric field lines. Because of the high resistance of the antenna terminals due to a small thickness of the gold film, most of the electric field is within the antenna terminals instead of between the antenna terminals.

IV. Future improvements

In order to observe the predicted effect of photon-assisted quantum transport, we need to enhance the quantum process and minimize the thermal effect. Several steps should be taken to achieve this goal:

1. Study the response of the quantum point contact devices at frequencies much higher than 300 GHz. Since the width of the photon-induced ministeps is proportional to the radiation frequency, these ministep structures will be more profound at higher frequencies. For example, at 1 THz, the photon energy $\hbar\omega = 4$ meV, which is comparable to the intersubband spacing between the first few subbands. Thus, the width of the photon-induced ministeps will be about the same as that of the original quantized conductance steps, and they should be quite distinctive, compared to thermal broadening. In addition, the dissipation in the 2DEG is proportional to ω^{-2}, thus heating will be substantially reduced at higher frequencies.
2. Using samples with higher electron mobilities ($\mu \approx 10^6$ cm^2/V•sec). The dissipation in the 2DEG is inversely proportional to the square of the scattering time τ (which is proportional to the electron mobility μ). The heating effect will be reduced in samples with higher electron mobilities.
3. Using thicker (~2000 Å) antenna terminals. This is perhaps the most important step to take in order to observe the effect of photon-assisted quantum transport. According to the theoretical discussions in Section II, it is crucial to concentrate the radiation field near the classical turning points, which are only several hundred angstroms from the center of the point contacts. Antennas made of high-conductivity films with thicknesses greater than the skin depths are required to achieve this goal. Thus, thick (~2000 Å) PMMA photoresist layers will be required to lift off thick metal films. This will require some experimentation since the electron scattering in thick resist layers will alter fine features of the devices. An alternative approach is to use x-ray lithography to fabricate the devices. The scattering of x-ray photons in resist is negligible, thus a thick layer of resist can be used to lift off thick metal layers. Given the relatively relaxed tolerance for our devices (the distance between the split-gate electrodes can range from 0.15 to 0.3 μm), we believe that high-quality devices with desired properties can be fabricated using the existing technologies.

In summary, we have fabricated several antenna-coupled quantum point contact devices which showed good dc transport characteristics. We have observed photon-induced drain/source current when the device is irradiated with coherent radiation at 285 GHz. Our analysis suggests that the observed photon-induced current is mainly due to heating or a bolometric effect. Our analysis has also identified a device defect (the antenna/gate electrodes are too thin) which suppressed the photon-assisted quantum transport process and pointed out several improvements need to be made. Our theoretical calculation has shown that the current responsivity of an antenna-coupled quantum point contact can approach the quantum efficiency $e/\hbar\omega$ at and above one THz.

This work was supported by NSF grants 9109330-ECS and DMR-9022933 at MIT, and was performed in part at the National Nanofabrication Facility which is supported by the National Science Foundation under Grant ECS-8619049, Cornell University, and industrial affiliates.

References

1. Qing Hu, Appl. Phys. Lett. **62**, 837 (1993).
2. B.J. van Wees, H. van Houten, C.W.J. Beenakker, J.G. Williamson, L.P. Kouwenhoven, D. van der Marel, and C.T. Foxon, Phys. Rev. Lett. **60**, 848 (1988).

3. D.A. Wharam, T.J. Thornton, R. Newbury, M. Pepper, H. Ajmed, J.E.F. Frost, D.G. Hasko, D.C. Peacock, D.A. Ritchie, and G.A. C. Jones, J. Phys. C **21**, L209 (1988).
4. C. W. J. Beenakker and H. van Houten, in *Solid State Physics*, vol. 44, Edited by H. Ehrenreich and D. Turnbull, (Academic, New York, 1991), pp. 1-228, and references therein.
5. P.L. Richards and Qing Hu, IEEE Proceedings, **77**, 1233 (1989).
6. Y. Imry, in *Directions in Condensed Matter Physics*, edited by G. Grinstein and G. Mazenko (World Scientific, 1986), pp. 101-164.
7. Shechao Feng and Qing Hu, submitted to Phys. Rev. **B**, February 1993.
8. P.K. Tien and J.P. Gordon, Phys. Rev. **129**, 647 (1963).
9. P.F. Bagwell and T.P. Orlando, Phys. Rev. **B40**, 1456 (1989); P.F. Bagwell and T. P. Orlando, Phys. Rev. **B40**, 3735 (1989).
10. D. B. Rutledge, D. P. Neikirk, and D. P. Kasilingam, in *Infrared and Millimeter Waves*, Edited by K. J. Button (Academic, New York, 1983), pp. 1-90.
11. M. J. Rooks, C. C. Eugster, J. A. del Alamo, G. Snider, and E. Hu, J. Vac. Sci. Technol. **B9**, 2856 (1991).